

Highly selective liquid-phase aerobic oxidation of vanillyl alcohol to vanillin on cobalt oxide (Co₃O₄) nanoparticles†

Cite this: *New J. Chem.*, 2013, **37**, 2669

Ajay Jha and Chandrashekhar V. Rode*

Received (in Porto Alegre, Brazil)
13th May 2013,
Accepted 4th June 2013

DOI: 10.1039/c3nj00508a

www.rsc.org/njc

Spinel Co₃O₄ nanoparticles prepared by solution phase method having particle size in the range of 12–20 nm exhibited excellent activity for the liquid-phase aerobic oxidation of vanillyl alcohol with 80% conversion and 98% selectivity to vanillin. Our catalyst could be reused three times without appreciable loss in activity. The catalytic activity of the Co₃O₄ nanoparticles was found to be similar to its homogenous precursor (cobalt acetate) and greater than the commercial Co₃O₄ oxide. The detailed characterization results of morphology, size and structure of the prepared Co₃O₄ nanoparticles obtained by XRD, FT-IR, H₂-TPR, HR-TEM and cyclic voltammetry technique were used to understand the roles of various Co species in directing the selectivity towards vanillin.

1 Introduction

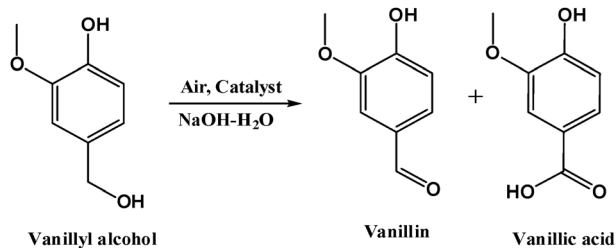
A great deal of research is focused on designing heterogeneous catalysts for liquid-phase aerobic oxidation for developing ecologically sustainable processes for fine chemicals.^{1,2} Liquid-phase aerobic oxidations provide a green route as aerial O₂ is one of the cheapest and greenest oxidants available and water is the only by-product formed.^{3–5} A major challenge for liquid-phase air oxidation is the activation of molecular oxygen under mild conditions to achieve the highest selectivity to the desired products. Although homogeneously catalyzed liquid-phase air oxidations are commonly practiced in industry using organometallic complexes as catalysts, the major drawbacks of such oxidations are: (i) poor selectivity to the desired product, a variety of oxygenated products are formed because of the formation of free radical intermediates; (ii) fast deactivation of homogeneous catalysts due to formation of μ -oxo dimers; (iii) contamination of the product due to trace metal impurities during catalyst separation protocol.^{6–9} These problems can be overcome by designing a suitable heterogeneous catalyst because they offer many advantages over their homogenous counterparts such as easy handling, separation and reusability. Therefore, development of functionalized heterogeneous catalysts is highly desirable

from an environmental point of view. Several noble metal-based heterogeneous catalysts such as Au/CeO₂, Pt/C, Ru/TiO₂ *etc.* have been explored for this purpose and such reactions are mediated by the use of alkali.^{10–13} Although noble metal catalysts exhibit high activity for oxidation reactions, they can be expensive, minimizing their potential for commercial applications.¹⁴ Oxides of other transition metals, such as copper, cobalt, manganese, and chromium, are also known to be effective catalysts for oxidation reactions.

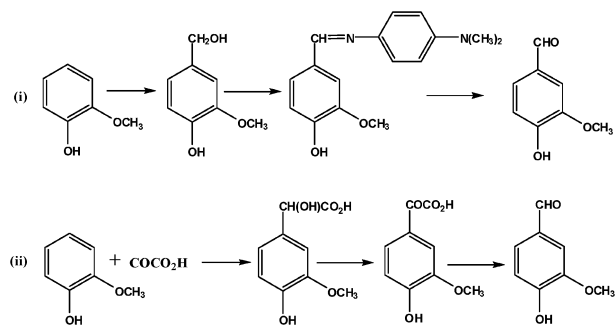
Among these metals, cobalt is the most attractive because of its strong capability for dioxygen activation (through metal–O₂ adduct formation) and because it is more cost effective compared to noble metals. As compared to their bulk counterparts, generally, nanostructured materials are more efficient as catalysts due to increased number of corner and edge atoms with decreasing the crystal domains, leading to higher adsorption rates and activation of the reactants.^{15,16} Hence, this work was undertaken to further explore and understand the mechanism by which nanostructured materials govern their performance, especially their role in directing the selectivity pattern in a consecutive oxidation reaction. For this purpose, we prepared Co₃O₄ nanoparticles by solution-phase method and investigated its catalytic performance for aerobic oxidation of vanillyl alcohol in the liquid phase (Scheme 1). Vanillin has major applications in the food and perfumery sectors because of its flavour and it also finds use in medicinal applications serving as a platform chemical for pharmaceutical production.¹⁷ Traditionally, vanillin was synthesized from guaiacol through (i) the nitroso, and (ii) the glyoxylic method.^{18,19} (Scheme 2).

Chemical Engineering & Process Development Division, CSIR-National Chemical Laboratory, Pune 411008, India. E-mail: cv.rode@ncl.res.in;
Fax: +91 20 2590 2621; Tel: +91 20 2590 2349

† Electronic supplementary information (ESI) available. See DOI: 10.1039/c3nj00508a



Scheme 1 Aerobic oxidation products of vanillyl alcohol.



Scheme 2 Traditional methods of vanillin synthesis. (i) Nitroso and (ii) glyoxylic methods.

Though these methods gave higher selectivity to vanillin, the formation of undesirable side products (nitrile and *p*-aminodimethyl aniline) in the case of the nitroso method, and the use of toxic oxidants (CuO, PbO₂ and MnO₂) in case of the glyoxylic method, and lower product yields (57%) are the serious drawbacks of these methods.²⁰

Here, we report the synthesis and characterization of Co₃O₄ nanoparticles and their use as catalysts for the aerobic liquid-phase oxidation of vanillyl alcohol to vanillin. The reusability of the catalyst was also demonstrated by the thermal regeneration steps during the catalyst recycle study. To the best of our knowledge, ours is the first report on highly selective Co₃O₄ nanoparticles for the liquid-phase aerobic oxidation of vanillyl alcohol to vanillin.

2 Experimental

2.1 Synthesis and characterization of Co₃O₄ nanoparticles

Co₃O₄ nanoparticles were prepared by solution-phase method as described earlier.²¹ In a typical synthesis, 4.98 g of cobalt acetate tetrahydrate was dissolved in 60 mL of ethylene glycol and the solution was gradually heated to 160 °C. To this, 200 mL of aqueous 0.2 M Na₂CO₃ solution was added dropwise and the slurry was further aged for 1 h under nitrogen atmosphere. The resulting solid was filtered, thoroughly washed with distilled water until neutralization, and dried overnight at 100 °C, then calcined at 450 °C for 4 h.

X-Ray diffractograms (XRD) of the catalysts were recorded in the 2θ range of 10–80° (scan rate of 5.3° min⁻¹) on a PANalytical PXRD Model X-Pert PRO-1712, using Ni-filtered Cu Kα radiation (λ = 0.154 nm) as a source (current intensity, 30 mA; voltage, 40 kV)

and an Xcelerator detector. Temperature programmed reduction (TPR) experiments were carried on a Micromeritics Chemisorb 2720 instrument. For this purpose, 0.02 g of the catalyst was placed in a quartz tube and treated with He gas (25 mL min⁻¹) at 200 °C for 1 h. A gas mixture of 5% hydrogen in argon was then passed through the quartz reactor at 50 °C for 1 h. The temperature was raised from room temperature to 900 °C at a heating rate of 10 °C min⁻¹ and held at 900 °C for 10 min.

2.2 Catalytic activity measurement

All the catalytic oxidation reactions were carried out in a 300 cm³ capacity high-pressure Hastelloy reactor supplied by Parr Instruments Co., U.S.A. The reactor was connected to an air reservoir held at a pressure higher than that of the reactor. Thermo Scientific HPLC model AS3000 liquid chromatograph equipped with an ultraviolet detector was used for the analysis. HPLC analysis was performed on a 25 cm RP-18 column. The products and reactant were detected using a UV detector at λ_{max} = 254 nm. Aqueous methanol (35%) was used as a mobile phase at a column temperature of 35 °C and a flow rate of 0.7 mL min⁻¹.

In a typical experiment, 0.5 g of NaOH and 70 mL of isopropanol were heated in a flask with a reflux condenser until the NaOH dissolved completely. This NaOH solution was charged with 0.5 g of vanillyl alcohol and 0.1 g catalyst into a 300 mL Parr autoclave. The reaction mixture was heated to 80 °C. After the desired temperature was attained, the reactor was pressurized with 6.8 bar air. Then the reaction was started by agitating the contents at 1000 rpm and was continued for 6 h. After 6 h, the reactor was cooled to room temperature and the unabsorbed air was vented out. Then the contents of the reactor were discharged and the final volume was recorded.

3 Results and discussion

3.1 Structural properties of Co₃O₄ nanoparticles

XRD diffractograms of the uncalcined and calcined samples of the prepared nano Co₃O₄ and commercial Co₃O₄ are displayed in Fig. 1. The as-synthesized material showed broad and asymmetric peaks at 2θ ~ 17.2, 33.6 and 39.3°, which are characteristic of the cobalt hydroxycarbonate phase.²² However, the diffractogram of the calcined sample was completely different from the as-synthesized sample. The broad XRD diffraction peaks observed for calcined Co₃O₄ oxide at 2θ ~ 19, 31.4, 36.9, 44.9, 59.5 and 65.4°, were ascribed to the cubic phase of the Co₃O₄ (JCPDS No. 74-1657). The average crystallite size of Co₃O₄ nanoparticles estimated from the full width at half maximum of the 311 diffraction peak by applying the Scherrer equation was about 14 nm, which was much smaller (six times) than that observed for the commercial Co₃O₄ (86 nm). The broader XRD diffraction peaks observed for our Co₃O₄ oxide indicate the nanocrystalline nature of the prepared catalyst.

The various cobalt oxide species possibly formed during the preparation of Co₃O₄ spinel were postulated from the temperature-programmed reduction analysis (TPR). The TPR profiles of Co₃O₄ showed a two step reduction process initiated at

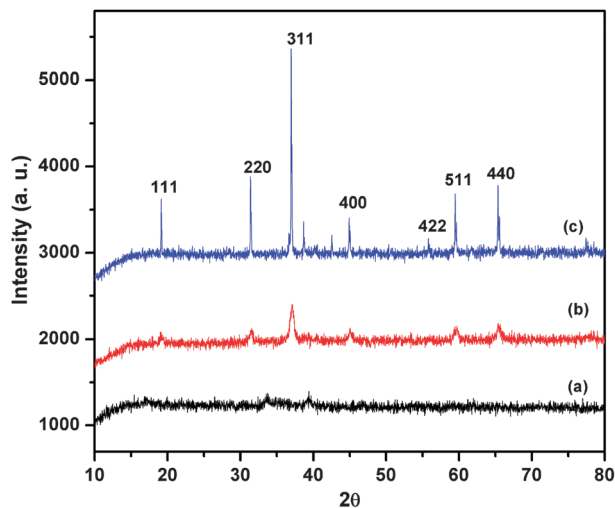


Fig. 1 XRD patterns of (a) the as-synthesized cobalt hydroxy carbonate, (b) Co_3O_4 nanoparticles, and (c) commercial Co_3O_4 .

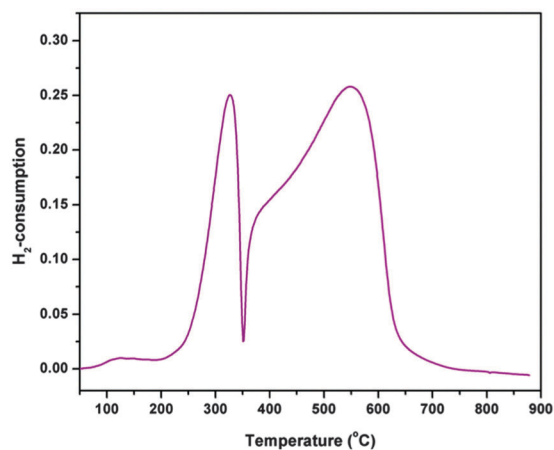
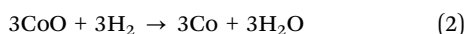
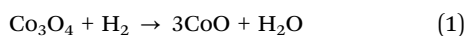


Fig. 2 H_2 -TPR profile of Co_3O_4 nanoparticles.

approximately 200 °C as shown in Fig. 2. The first reduction peak was very sharp and symmetrical and the temperature maximum was centred at about 325 °C. This peak was associated with the reduction of trivalent cobalt oxide (Co_3O_4) to divalent cobalt oxide (CoO) (eqn (1)). The second reduction peak was broad and unsymmetrical with the temperature maxima centred at about 548 °C. This could be attributed to the subsequent reduction of divalent cobalt oxide (CoO) to metallic cobalt (Co°).^{23,24} (eqn (2))



The amount of hydrogen consumed at low temperature (325 °C) was about one third (3.83 mmol g^{-1}) of that for the higher temperature (548 °C, 11.8 mmol g^{-1}). The ratio of hydrogen consumed between the 1st and 2nd peaks was close to 1:3, which is consistent with the stoichiometry of Co_3O_4 reduction. The reduction of CoO to metallic Co was strongly

dependent on the morphology of Co_3O_4 . As reported earlier, in case of the nanoparticles, the reduction of CoO to Co metal started at 400 °C and was completed at 550 °C, while for nanotube morphology, it started from 500 °C and completed at 650 °C. However in our case, CoO reduction started at 350 °C and was completed at around 650 °C. This observation clearly shows that the prepared Co_3O_4 existed with mixed nanocomposite morphology giving an unsymmetrical reduction peak as observed during reduction of CoO to metallic Co (Fig. 2). HR-TEM images (discussed later, Fig. 4) also suggest the mixed nanocomposite morphology of the prepared Co_3O_4 spinel.

Formation of Co_3O_4 spinel was also evident from the FT-IR characterization. Fig. 3 shows the FTIR spectra of the as-synthesized material (cobalt hydroxycarbonate) and Co_3O_4 nanoparticles. As compared with the cobalt hydroxyl carbonate, the IR spectrum of the Co_3O_4 nanoparticles displayed two sharp bands at 563 and 667 cm^{-1} , originating from the stretching vibration of the metal–oxygen bonds. On the basis of earlier reports,^{25,26} the former band at 563 cm^{-1} was attributed to Co^{3+} in an octahedral hole and the latter band at 667 cm^{-1} for Co^{2+} in a tetrahedral hole. The fingerprint of IR absorption at 563 and 667 cm^{-1} for the Co_3O_4 spinel was fully developed after calcination at 450 °C.

Fig. 4 shows HR-TEM images of Co_3O_4 nanoparticles synthesized by the solution phase method and subsequent calcination at 450 °C. The as-synthesized material had a fully developed rod-like morphology (Fig. 4a), while the calcined nanoparticles showed a mixed morphology which included cubic, tubular and truncated polyhedron shapes (Fig. 4b). These cobalt oxide nanoparticles were arranged in chain-like fashion with particle size ranging from 12–20 nm, which matched well with the crystallite size calculated from XRD. The fringe patterns of the prepared Co_3O_4 nanoparticles obtained by HR-TEM are shown in Fig. 4c. According to this, the dominant exposed planes were (111) with a lattice space of 0.46 nm. The other exposed planes observed were (220) and (311) with lattice spaces of 0.28 and 0.24 nm, respectively. Fig. 4d shows the cross-section view near the (110) orientation exhibiting a rectangular shape with a long

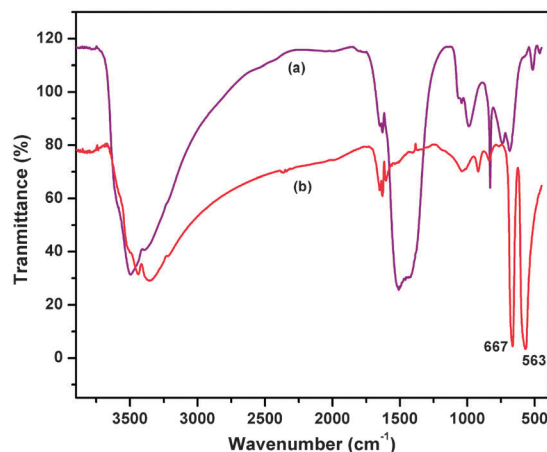


Fig. 3 FT-IR spectra for (a) cobalt hydroxycarbonate, and (b) Co_3O_4 nanoparticles.

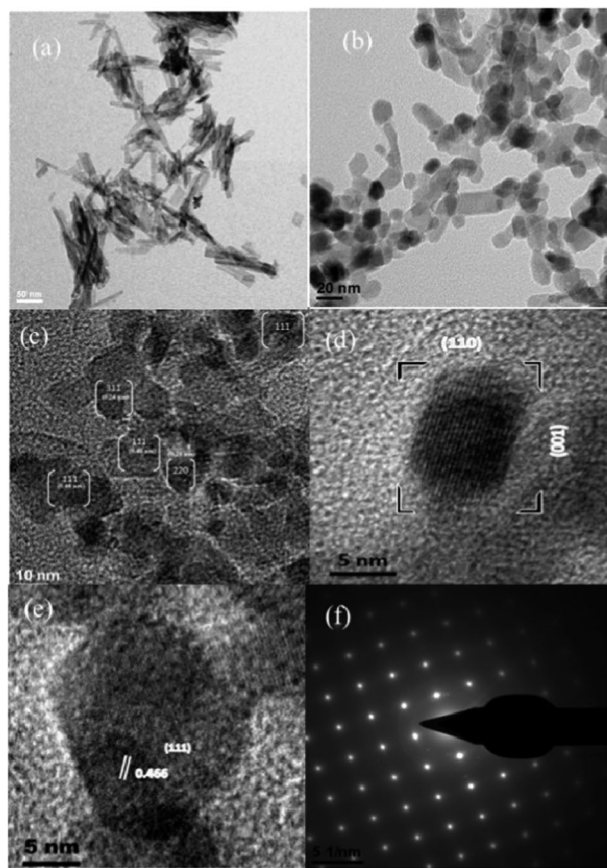


Fig. 4 (a–e) HR-TEM images of Co_3O_4 nanoparticles and (f) SAED pattern of Co_3O_4 nanoparticles.

edge parallel to (001). These 001 planes were constructed from (220) planes. Selected area ED analysis was also carried out to understand the crystallographic orientation of the Co_3O_4 nanocrystallites. Fig. 4f displayed the ED patterns of the cube present in the Co_3O_4 nanocomposite. The lattice constants obtained from the ED patterns are in excellent agreement with those from the XRD analysis.

The active sites present in Co_3O_4 could be approximately estimated by the $\text{Co}^{3+}/\text{Co}^{4+}$ redox profiles obtained by cyclic voltammetry (CV). CV measurements were performed at a scan rate of 50 mV s^{-1} over the potential range of 0–0.6 V in 0.1M KOH solution by using a quasi reference electrode. As can be seen in Fig. 5, during the positive scanning a broad hump was observed, which could be associated with the oxidation of Co^{3+} on the surface of Co_3O_4 .

Corresponding to the oxidation process, a similar broad hump was observed at the cathode near 0.45 V, which was attributed to the reduction of Co^{4+} to Co^{3+} .²⁷ The broad peak may be due to the mixed morphology of Co_3O_4 , as it was also confirmed by H_2 -TPR and HR-TEM measurements.

These results are characteristic of the surface confined redox couple as shown by the reaction in Fig. 5. Morphology and crystallite size of the Co_3O_4 has a significant influence on the exposed number of Co^{3+} species. From the integrated area of the Co^{3+} oxidation peaks shown in Fig. 5, it could be evaluated

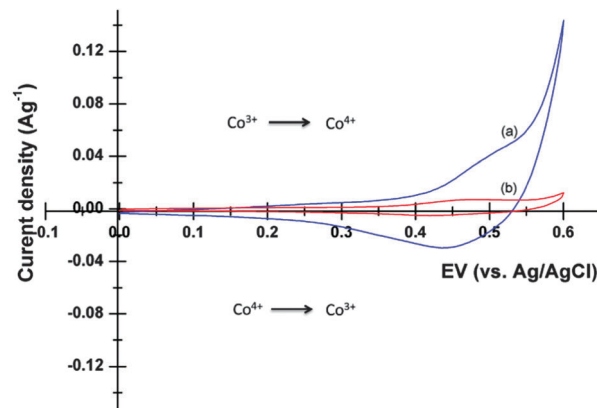


Fig. 5 CV curve in 0.1 M KOH solution of (a) prepared Co_3O_4 and (b) commercial Co_3O_4 .

that the exposed surface area of Co^{3+} in Co_3O_4 was higher in our nano Co_3O_4 sample than in the commercial Co_3O_4 sample. The area of the oxidation–reduction peak for the commercial Co_3O_4 sample was very much less, which was attributed to its higher crystallite size.

3.2 Catalytic performance of Co_3O_4 nanoparticles

The comparison of the activity and selectivity of different catalysts for the liquid-phase air oxidation of vanillyl alcohol is shown in Table 1. All the reactions were performed under optimum reaction conditions in alkaline medium except entry 4. The role of base is probably to deprotonate the phenolic –OH to form the phenoxy anion, which is the reactive species and favours coordination to the cobalt(III) species, increasing the activity.²⁸ Oxidation of vanillyl alcohol in an alkaline medium without catalyst did not show any activity. However, oxidation of vanillyl alcohol in the presence of catalyst and a base led to the selective formation of vanillin (98%), with 80% conversion of vanillyl alcohol. This could be possible by active participation of the Co^{3+} species. As observed in the HR-TEM images of the material, the presence of (110) plane was revealed. According to Xie *et al.*, (110) planes of Co_3O_4 are a characteristic of Co^{3+} species, which is the active component for the oxidation reaction. A comparable oxidation activity of the homogeneous precursor was also observed (entry 1, Table 1), but it suffers a major problem of difficult recovery and then recyclability. A control experiment with commercial Co_3O_4 gave a much lower conversion (45%) with almost the same selectivity pattern as shown in Table 1 (entry 3). The lower activity of the commercial Co_3O_4

Table 1 Catalyst screening for liquid-phase aerobic oxidation of vanillyl alcohol

Entry	Catalyst	Conversion (%)	Selectivity (%)	
			Vanillin	Vanillic acid
1	$\text{Co}(\text{ac})_2^a$	82	96	4
2	Co_3O_4 nanoparticles	80	98	2
3	Commercial Co_3O_4	45	98	2
4	Co_3O_4 nanoparticles ^b	25	88	12

^a Homogeneous catalyst. ^b Reaction without NaOH.

was due to its higher crystallite size (86 nm), which would offer less Co(III) active species for the oxidation, as is also supported by its CV measurement. In addition, the surface area of nanosize Co_3O_4 was found to be $87 \text{ m}^2 \text{ g}^{-1}$, about 17 times higher than that of the commercial Co_3O_4 sample ($5 \text{ m}^2 \text{ g}^{-1}$). Secondly, the lattice fringe patterns of nano Co_3O_4 showed the presence of the (111) plane, which was absent in the commercial Co_3O_4 , in which 'd' spacing of 0.28 nm was characteristic of the (220) plane (ESI,† S4). Hence both the factors *viz.* higher surface area as well as a dominant (111) plane exposing the active Co^{3+} sites of nano Co_3O_4 , are responsible for its higher specific activity. The TOF calculated for Co_3O_4 nanoparticles was 6.4 h^{-1} while that for commercial Co_3O_4 was 1.2 h^{-1} . Under the same reaction conditions, oxidation of vanillyl alcohol in the absence of a base leads to the lower conversion of vanillyl alcohol (25%) with 88% selectivity to vanillin and 12% vanillic acid, as shown in Table 1 (entry 4). It seems that in the oxidation of the vanillyl alcohol, the catalytic role of cobalt in the absence of base is weak but not absent because abstraction of the β -proton from the vanillyl alcohol depends on the formation of the superoxo-Co(III) species.²⁹

The effect of reaction time on vanillyl alcohol conversion and selectivity to vanillin was also studied for Co_3O_4 nanocatalyst and the results are shown in Fig. 6. The conversion of vanillyl alcohol increased from 49 to 80% with a consistent selectivity (98%) to vanillin. While an increase in reaction time from 2 to 6 h, conversion became low (86%) with a decrease in selectivity to vanillin from 98 to 94% in 8 h. The decrease in conversion and selectivity to vanillin might be due to the formation of polymeric materials over the catalyst surface as observed by the increase in the catalyst weight after the reaction.

In order to study the stability of this heterogeneous catalyst, its recycle experiments were carried out in the following way: after the first oxidation run with fresh Co_3O_4 catalyst, it was filtered out and washed several times with methanol, dried

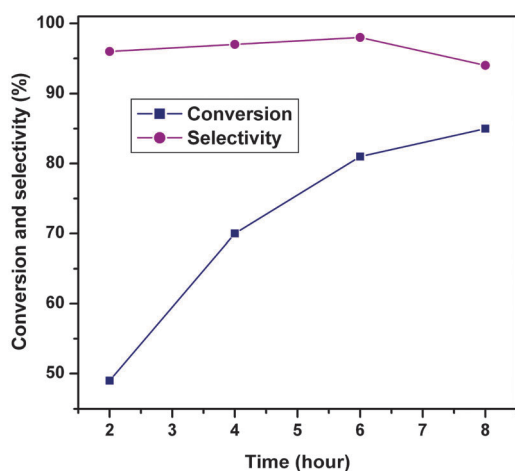


Fig. 6 Effect of time on conversion and selectivity. Reaction conditions: molar ratio of NaOH/vanillyl alcohol, 3.8; Co_3O_4 nanocatalyst (0.1 g), 353 K, iso-propyl alcohol (70 ml), O_2 -pressure (6.8 bar).

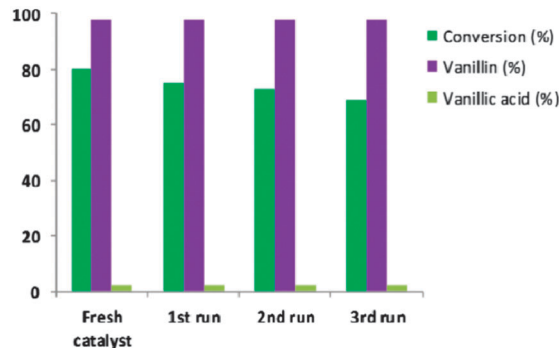


Fig. 7 Recycling study of vanillyl alcohol oxidation.

under vacuum at $100 \text{ }^\circ\text{C}$ for 2 h and then reused after calcination at $450 \text{ }^\circ\text{C}$ for 1 h. The procedure was followed for three subsequent oxidation experiments, and the results are shown in Fig. 7. The conversion of vanillyl alcohol was found to decrease from 80 to 69% after the 3rd recycle study, however, selectivity to vanillin remained constant (98%). XRD and HR-TEM image of the used catalyst after the 3rd recycle showed that the particle size of the catalyst remained intact while the morphology of the Co_3O_4 was changed from mixed morphology, which included cubic, tubular and truncated polyhedron, to roughly spherical shape (ESI,† S1 and S2). The decrease in the catalytic activity of the used catalyst might be due to the change in the morphology, which leads to the change in the crystal planes of the catalyst, which are responsible for exposing the active sites on the surface.³⁰ The selectivity of the product did not change during recycling of the catalyst. This implies that the morphology affects the reaction rate significantly but has no influence on the reaction pathway.

In order to eliminate the possibility of a homogeneously catalyzed reaction due to the dissolution of cobalt oxide, a leaching test was performed as follows. The nano Co_3O_4 catalyst was separated from the reaction mixture by simple filtration after a partial conversion of 45% in 2 h, and the filtrate was then continued for further reaction under similar conditions (6.8 bar air pressure at $80 \text{ }^\circ\text{C}$), which did not give any conversion. The absence of any cobalt species in the filtrate was also confirmed by inductively coupled plasma spectrometry. These results clearly support the fact that the oxidation of vanillyl alcohol, catalyzed by Co_3O_4 , is truly heterogeneous in nature.

4 Conclusions

In this work, Co_3O_4 nanoparticles were prepared by a solution phase method and its catalytic activity for liquid-phase aerobic oxidation of vanillyl alcohol was evaluated. Comparison between commercial and prepared Co_3O_4 for vanillyl alcohol oxidation showed that the prepared Co_3O_4 was a better catalyst for vanillyl alcohol oxidation. The higher activity of the prepared Co_3O_4 was due to its smaller crystallite size (14 nm), higher surface area ($87 \text{ m}^2 \text{ g}^{-1}$) and higher exposure of Co^{3+} species over the Co_3O_4 surface as confirmed by CV measurement.

The prepared material showed a mixed morphology of cubic, polyhedron and nanotube types, which was confirmed by HR-TEM. Catalytic activity of the prepared Co_3O_4 was similar to the homogeneous precursor; however, the heterogeneous catalyst could be successfully recycled three times for vanillyl alcohol oxidation. Further efforts to synthesize the material with uniform morphology and an investigation into its effects on catalytic oxidation reactions are in progress.

Notes and references

- V. S. Kshirsagar, A. C. Garade, K. R. Patil, R. K. Jha and C. V. Rode, *Ind. Eng. Chem. Res.*, 2009, **48**, 9423.
- R. K. Marella, C. K. P. Neeli, S. R. R. Kamaraju and D. R. Burri, *Catal. Sci. Technol.*, 2012, **2**, 1833.
- T. Mitsudome, A. Noujima, T. Mizugaki, K. Jitsukawa and K. Kaneda, *Adv. Synth. Catal.*, 2009, **351**, 1890.
- S. E. Davis, M. S. Ide and R. J. Davis, *Green Chem.*, 2013, **15**, 17.
- M. Lakshmi Kantama, R. S. Reddy, U. Pal, M. Sudhakar, A. Venugopal, K. J. Ratnam, F. Figueras and V. R. Chintareddy, *J. Mol. Catal. A: Chem.*, 2012, **359**, 1.
- V. D. Makwana, Y. C. Son, A. R. Howell and S. L. Suib, *J. Catal.*, 2002, **210**, 46.
- A. C. Garade, N. S. Biradar, S. M. Joshi, V. S. Kshirsagar, R. K. Jha and C. V. Rode, *Appl. Clay Sci.*, 2011, **53**, 157.
- V. S. Kshirsagar, A. C. Garade, K. R. Patil, M. Shirai and C. V. Rode, *Top. Catal.*, 2009, **52**, 784.
- G. C. Behera and K. M. Parida, *Appl. Catal., A*, 2012, **413–414**, 245.
- Y. Zhang, X. Cui, F. Shi and Y. Deng, *Chem. Rev.*, 2012, **112**, 2467.
- M. Martín-Hernández, J. Carrera, M. E. Suárez-Ojedaa, M. Besson and C. Descorme, *Appl. Catal., B*, 2012, **123–124**, 141.
- P. Haider, B. Kimmerle, F. Krumeich, W. Kleist, J. Grunwaldt and A. Baiker, *Catal. Lett.*, 2008, **125**, 169.
- Y. Shen, S. Zhang, H. Li, Y. Ren and H. Liu, *Chem.–Eur. J.*, 2010, **16**, 7368.
- U. Menon, V. V. Galvita and G. B. Marin, *J. Catal.*, 2011, **238**, 1.
- V. S. Kshirsagar, S. Vijayanand, H. S. Potdar, P. A. Joy, K. R. Patil and C. V. Rode, *Chem. Lett.*, 2008, **37**, 310.
- J. Zhu, K. Kailasam, A. Fischer and A. Thomas, *ACS Catal.*, 2011, **1**, 342.
- J. F. Stanzione, J. M. Sadler, J. J. La Scala, K. H. Reno and R. P. Wool, *Green Chem.*, 2012, **14**, 2346.
- A. D. Bulam, S. V. Nekrasov, B. V. Passet and V. G. Foshkin, *J. Appl. Chem.*, 1988, **61**, 859.
- S. R. Rao and G. A. Ravishankar, *J. Sci. Food Agric.*, 2000, **80**, 289.
- J. Hu, Y. Hu, J. Mao, J. Yao, Z. Chen and H. Li, *Green Chem.*, 2012, **14**, 2894.
- X. Xie, Y. Li, Z. Liu, M. Haruta and W. Shen, *Nature*, 2009, **458**, 746.
- R. Xu and H. C. Zeng, *J. Phys. Chem. B*, 2003, **107**, 12643.
- P. Arnoldy and J. A. Moulijn, *J. Catal.*, 1985, **93**, 38.
- W. J. Xue, Y. F. Wang, P. Li, Z. Liu, Z. P. Hao and C. Y. Ma, *Catal. Commun.*, 2011, **12**, 1265.
- J. Xu, P. Gaob and T. S. Zhao, *Energy Environ. Sci.*, 2012, **5**, 5333.
- Z. P. Xu and H. C. Zeng, *J. Mater. Chem.*, 1998, **8**, 2499.
- F. Svegli, B. Orel, I. Grabec-Svegli and V. Kaucic, *Electrochim. Acta*, 2000, **45**, 4359–4371.
- B. Barton, C. G. Logie, B. M. Schoonees and B. Zeelie, *Org. Process Res. Dev.*, 2005, **9**, 62.
- I. Fernández, J. R. Pedro, A. L. Roselló, R. Ruiz, I. Castro, X. Ottenwaelder and Y. Journaux, *Eur. J. Org. Chem.*, 2001, 1235.
- X. Xie and W. Shen, *Nanoscale*, 2009, **1**, 50–60.